arXiv:1511.06880v1 [cond-mat.mes-hall] 21 Nov 2015

Transmission via Triangular Double Barrier and Magnetic Fields in Graphene

Miloud Mekkaoui[a], **Ahmed Jellal**[*a,b] and **Hocine Bahlouli**[b,c]

[a] *Theoretical Physics Group, Faculty of Sciences, Chouaïb Doukkali University, PO Box 20, 24000 El Jadida, Morocco*

[b] *Saudi Center for Theoretical Physics, Dhahran, Saudi Arabia*

[c] *Physics Department, King Fahd University of Petroleum & Minerals, Dhahran 31261, Saudi Arabia*

Abstract

We study the transmission probability of Dirac fermions in graphene scattered by a triangular double barrier potential in the presence of an external magnetic field. Our system made of two triangular potential barrier regions separated by a well region characterized by an energy gap G_p. Solving our Dirac-like equation and matching the solutions at the boundaries we express our transmission and reflection coefficients in terms of transfer matrix. We show in particular that the transmission exhibits oscillation resonances that are manifestation of the Klein tunneling effect.

PACS numbers: 72.80.Vp, 73.21.-b, 71.10.Pm, 03.65.Pm
Keywords: graphene, double barriers, scattering, transmission.

[*] ajellal@ictp.it – a.jellal@ucd.ac.ma

1 Introduction

Graphene [1] remains among the most fascinating and attractive subject has been seen right now in condensed matter physics. This is because of its exotic physical properties and the apparent similarity of its mathematical model to the one describing relativistic fermions in two dimensions. As a consequence of this relativistic-like behavior particles could tunnel through very high barriers in contrast to the conventional tunneling of non-relativistic particles, an effect known in relativistic field theory as Klein tunneling. This tunneling effect has already been observed experimentally [2] in graphene systems. There are various ways for creating barrier structures in graphene [3, 4]. For instance, it can be done by applying a gate voltage, cutting the graphene sheet into finite width to create a nanoribbons, using doping or through the creation of a magnetic barrier. In the case of graphene, results of the transmission coefficient and the tunneling conductance were already reported for the electrostatic barriers [5–8], magnetic barriers [7, 9, 10], potential barrier [11, 13] and triangular barrier [14].

We study the transmission probability of Dirac fermions in graphene scattered by a triangular double barrier potential in the presence of an inhomogeneous magnetic fields B. We emphasis that B-field discussed in our manuscript is applied externally. It can be created for instance by depositing a type-I superconducting film on top of the system and remove a strip $|x| < d_1$ of the superconductor and apply a perpendicular magnetic field. This patterning technique of creating the desired magnetic field profile was proposed in [15]. One of the interesting features of such inhomogeneous magnetic field profile is that it can bind electrons, contrary to the usual potential step. Such a step magnetic field will indeed result in electron states that are bound to the step B-field and that move in one direction along the step. Thus there is a current along the y-direction but it is a very small effect and is not relevant for our problem (those electrons have $k_x = 0$). Indeed, we consider free electron states that have in general k_x non zero, because otherwise they will not tunnel. A recent work studied double barriers with magnetic field in graphene without mass term [16].

The paper is organized as follows. In section 2, we formulate our model by setting the Hamiltonian system describing particles scattered by a triangular double barrier whose well potential zone is subject to a magnetic field with a mass term. In section 3, we consider the case of static double barriers and derive the energy spectrum to finally determine the transmission and reflection probabilities. Their behaviors are numerically investigated and in particular resonances were seen in different regions as well as the Klein tunneling effect. In section 4, we study the same system but this time by taking into account the presence of an inhomogeneous magnetic field. Using boundary conditions, we split the energy into three domains and then calculate the transmission probability in each case. In each situation, we discuss the transmission at resonances that characterize each region and stress the importance of our results. We conclude our work in the final section.

2 Mathematical model

We consider a system of massless Dirac fermions incident on a two-dimensional strip of graphene having energy E and at incidence angle ϕ_1 with respect to the x-direction. This system is a flat sheet of graphene subject to a square potential barrier along the x-direction while particles are free in the

y-direction. Let us first describe the geometry of our system, which is made of five regions denoted by $\mathsf{j} = 1, \cdots, 5$. Each region is characterized by its constant potential and interaction with external sources. All regions are formally described by a Dirac-like Hamiltonian

$$H = v_F \boldsymbol{\sigma} \cdot \left(\mathbf{p} + \frac{e}{c} \mathbf{A} \right) + V(x) \mathbb{I}_2 + G_p \Theta \left(d_1^2 - x^2 \right) \sigma_z \tag{1}$$

where $v_F \approx 10^6 m/s$ is the Fermi velocity, $\boldsymbol{\sigma} = (\sigma_x, \sigma_y)$ and σ_z are the Pauli matrices in pseudospin space, $\mathbf{p} = -i\hbar(\partial_x, \partial_y)$ is the momentum operator, $\mathbb{I}_2$ the 2×2 unit matrix, $V(x) = V_{\mathsf{j}}$ is the electrostatic potential in the j-th scattering region and Θ is the Heaviside step function. The magnetic field $B(x, y) = B(x)$ is defined through the Landau gauge, which allows the vector potential to be of the form $\mathbf{A} = (0, A_y(x))$ with $\partial_x A_y(x) = B(x)$. The parameter $G_p = m v_F^2$ is the energy gap owing to the sublattice symmetry breaking, it can also be seen as the energy gap $G_p = G_{p,so}$ originating from spin-orbit interaction.

First let us specify potential configuration that will constitute our double barrier potential

$$V(x) = \begin{cases} \Lambda(d_2 + \gamma x), & d_1 \leq |x| \leq d_2 \\ V_2, & |x| \leq d_1 \\ 0, & \text{otherwise} \end{cases} \tag{2}$$

where $\gamma = \pm 1$, $\gamma = 1$ for $x \in [-d_2, -d_1]$, $\gamma = -1$ for $x \in [d_1, d_2]$ and the parameter Λ defined by $\Lambda = \frac{V_1}{d_2 - d_1}$ gives the slope of triangular potentials. The graphical representation of this potential is shown in Figure 1. We define each potential region as follows: $\mathsf{j} = 1$ for $x \leq -d_2$, $\mathsf{j} = 2$ for $-d_2 \leq x \leq -d_1$, $\mathsf{j} = 3$ for $-d_1 \leq x \leq d_1$, $\mathsf{j} = 4$ for $d_1 \leq x \leq d_2$ and $\mathsf{j} = 5$ for $x \geq d_2$. The corresponding constant potentials are defined by (2) and are denoted by V_j in the j-th region.

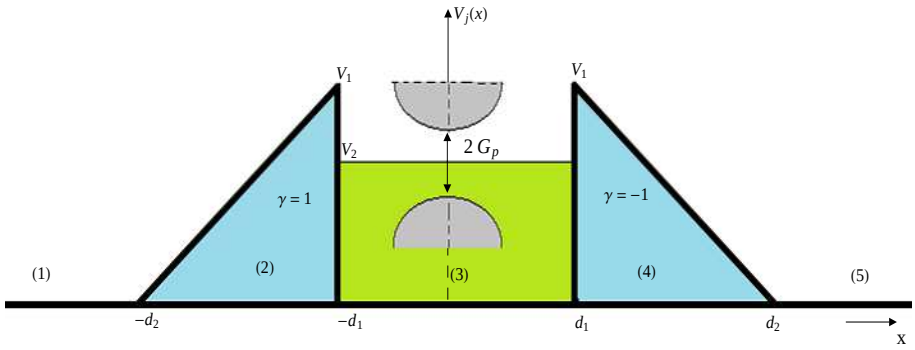

Figure 1: Schematic diagram for the monolayer graphene double barrier.

3 Static double barrier

We consider the Hamiltonian describing Dirac fermions in graphene scattered by an electrostatic double barrier potential without magnetic field $\mathbf{A} = 0$. In this case (1) reduces to

$$H_s = v_F \boldsymbol{\sigma} \cdot \mathbf{p} + V(x) \mathbb{I}_2 + G_p \Theta \left(d_1^2 - x^2 \right) \sigma_z \tag{3}$$

where j labels the five regions indicated schematically in Figure 1 showing the space configuration of the potential profile. Due to sublattice symmetry we therefore need to study our system only near the **K** point. The time-independent Dirac equation for the spinor $\Phi(x,y)=(\varphi^{+},\varphi^{-})^{T}$ at energy $E=v_F\epsilon$ then reads, in the unit system $\hbar=m=c=1$, as

$$\left[\boldsymbol{\sigma}\cdot\mathbf{p}+v_j\mathbb{I}_2+\mu\Theta\left(d_1^2-x^2\right)\sigma_z\right]\Phi(x,y)=\epsilon\Phi(x,y) \tag{4}$$

where $V_{\mathsf{j}}=v_F v_{\mathsf{j}}$ and $G_p=v_F\mu$. Our system is supposed to have finite width W with infinite mass boundary conditions on the wavefunction at the boundaries $y=0$ and $y=W$ along the y-direction [17, 18]. These boundary conditions result in a quantization of the transverse momentum along the y-direction as

$$k_y=\frac{\pi}{W}\left(n+\frac{1}{2}\right),\qquad n=0,1,2\cdots. \tag{5}$$

One can therefore assume a spinor solution of the following form $\Phi_{\mathsf{j}}=\left(\varphi_{\mathsf{j}}^{+}(x),\varphi_{\mathsf{j}}^{-}(x)\right)^{\dagger}e^{ik_y y}$ and the subscript $\mathsf{j}=1,2,3,4,5$ indicates the space region while the superscripts indicate the two spinor components. Solving the eigenvalue equation to obtain the upper and lower components of the eignespinor in the incident and reflection region 1 ($x<-d_2$)

$$\Phi_{\mathsf{1}}=\begin{pmatrix}1\\ z_1\end{pmatrix}e^{i(k_1x+k_yy)}+r_{s,n}\begin{pmatrix}1\\ -z_1^{-1}\end{pmatrix}e^{i(-k_1x+k_yy)} \tag{6}$$

$$z_1=s_1\frac{k_1+ik_y}{\sqrt{k_1^2+k_y^2}} \tag{7}$$

where the sign function is defined by $s_{\mathsf{j}}=\mathrm{sign}(E)$. The corresponding dispersion relation takes the form

$$\epsilon=s_1\sqrt{k_1^2+k_y^2}. \tag{8}$$

In regions 2 and 4 ($d_1<|x|<d_2$), the general solution can be expressed in terms of the parabolic cylinder function [14, 19, 20] as

$$\chi_\gamma^{+}=c_{n1}D_{\nu_n-1}\left(Q_\gamma\right)+c_{n2}D_{-\nu_n}\left(-Q_\gamma^{*}\right) \tag{9}$$

where c_{n1} and c_{n2} are constants, $\nu_n=\frac{ik_y^2}{2\varrho}$ and $Q_\gamma(x)=\sqrt{\frac{2}{\varrho}}e^{i\pi/4}\left(\gamma\varrho x+\epsilon_0\right)$, with $\epsilon_0=\epsilon-v_1$, $\Lambda=v_F\varrho$, $V_1=v_Fv_1$. The lower spinor component is given by

$$\chi_\gamma^{-}=-\frac{c_{n2}}{k_y}\left[2(\epsilon_0+\gamma\varrho x)D_{-\nu_n}\left(-Q_\gamma^{*}\right)+\sqrt{2\varrho}e^{i\pi/4}D_{-\nu_n+1}\left(-Q_\gamma^{*}\right)\right]-\frac{c_{n1}}{k_y}\sqrt{2\varrho}e^{-i\pi/4}D_{\nu_n-1}\left(Q_\gamma\right). \tag{10}$$

The components of the spinor solution of the Dirac equation (4) in regions 2 and 4 can be obtained from (9) and (10) with $\varphi_\gamma^{+}(x)=\chi_\gamma^{+}+i\chi_\gamma^{-}$ and $\varphi_\gamma^{-}(x)=\chi_\gamma^{+}-i\chi_\gamma^{-}$. Then, in regions 2 and 4 we have the eigenspinors

$$\Phi_{\mathsf{j}}\;=\;a_{\mathsf{j}-1}\begin{pmatrix}\eta_\gamma^{+}(x)\\ \eta_\gamma^{-}(x)\end{pmatrix}e^{ik_yy}+a_{\mathsf{j}}\begin{pmatrix}\xi_\gamma^{+}(x)\\ \xi_\gamma^{-}(x)\end{pmatrix}e^{ik_yy} \tag{11}$$

where the functions $\eta_\gamma^{\pm}(x)$ and $\xi_\gamma^{\pm}(x)$ are given by

$$\eta_\gamma^{\pm}(x)=D_{\nu_n-1}\left(Q_\gamma\right)\mp\frac{1}{k_y}\sqrt{2\varrho}e^{i\pi/4}D_{\nu_n}\left(Q_\gamma\right) \tag{12}$$

$$\xi_\gamma^{\pm}(x)=\pm\frac{1}{k_y}\sqrt{2\varrho}e^{-i\pi/4}D_{-\nu_n+1}\left(-Q_\gamma^{*}\right)\pm\frac{1}{k_y}\left(-2i\epsilon_0\pm k_y-\gamma 2i\varrho x\right)D_{-\nu_n}\left(-Q_\gamma^{*}\right). \tag{13}$$

More explicitly, it gives in region 2

$$\Phi_2 = a_1 \begin{pmatrix} \eta_1^+(x) \\ \eta_1^-(x) \end{pmatrix} e^{ik_y y} + a_2 \begin{pmatrix} \xi_1^+(x) \\ \xi_1^-(x) \end{pmatrix} e^{ik_y y} \tag{14}$$

and region 4

$$\Phi_4 = a_3 \begin{pmatrix} \eta_{-1}^+(x) \\ \eta_{-1}^-(x) \end{pmatrix} e^{ik_y y} + a_4 \begin{pmatrix} \xi_{-1}^+(x) \\ \xi_{-1}^-(x) \end{pmatrix} e^{ik_y y} \tag{15}$$

where $\gamma = \pm 1$.

Solving the eigenvalue equation for the Hamiltonian (4) in region 3, we find the following eigenspinor

$$\Phi_3 = b_1 \begin{pmatrix} \alpha \\ \beta z_3 \end{pmatrix} e^{i(k_3 x + k_y y)} + b_2 \begin{pmatrix} \alpha \\ -\beta z_3^{-1} \end{pmatrix} e^{i(-k_3 x + k_y y)} \tag{16}$$

$$z_3 = s_3 \frac{k_3 + i k_y}{\sqrt{k_3^2 + k_y^2}} \tag{17}$$

where the parameters α and β are defined by

$$\alpha = \left(1 + \frac{\mu}{\epsilon - v_2}\right)^{1/2}, \qquad \beta = \left(1 - \frac{\mu}{\epsilon - v_2}\right)^{1/2} \tag{18}$$

with the sign function $s_3 = \text{sign}(\epsilon - v_2)$. The wave vector being

$$k_3 = \sqrt{(\epsilon - v_2)^2 - \mu^2 - {k_y}^2}. \tag{19}$$

Finally the eigenspinor in region 5 can be expressed as

$$\Phi_5 = t_{s,n} \begin{pmatrix} 1 \\ z_1 \end{pmatrix} e^{i(k_1 x + k_y y)}. \tag{20}$$

The transmission and reflection coefficients $(r_{s,n}, t_{s,n})$ can be determined using the boundary conditions, that is, continuity of the eigenspinors at each interface. Next we will use the above solutions to explicitly determine the corresponding coefficient. Now, requiring the continuity of the spinor wavefunctions at each junction interface gives rise to the following set of equations

$$\Phi_1(-d_2) = \Phi_2(-d_2) \tag{21}$$

$$\Phi_2(-d_1) = \Phi_3(-d_1) \tag{22}$$

$$\Phi_3(d_1) = \Phi_4(d_1) \tag{23}$$

$$\Phi_4(d_2) = \Phi_5(d_2). \tag{24}$$

We prefer to express these relationships in terms of 2×2 transfer matrices between different regions. For this, we write

$$\begin{pmatrix} a_{\mathrm{j}} \\ b_{\mathrm{j}} \end{pmatrix} = M_{\mathrm{j,j+1}} \begin{pmatrix} a_{\mathrm{j+1}} \\ b_{\mathrm{j+1}} \end{pmatrix} \tag{25}$$

where $M_{\mathrm{j,j+1}}$ being the transfer matrices that couple the wavefunction in the j-th region to the wavefunction in the $\mathrm{j}+1$-th region. Finally, we obtain the full transfer matrix over the whole double barrier which can be written, in an obvious notation, as follows

$$\begin{pmatrix} 1 \\ r_{s,n} \end{pmatrix} = \prod_{\mathrm{j}=1}^{4} M_{\mathrm{j,j+1}} \begin{pmatrix} t_{s,n} \\ 0 \end{pmatrix} = M \begin{pmatrix} t_{s,n} \\ 0 \end{pmatrix} \tag{26}$$

where the total transfer matrix $M = M_{12} \cdot M_{23} \cdot M_{34} \cdot M_{45}$ is given by

$$M = \begin{pmatrix} m_{11} & m_{12} \\ m_{21} & m_{22} \end{pmatrix} \tag{27}$$

$$M_{12} = \begin{pmatrix} e^{-ik_1 d_2} & e^{ik_1 d_2} \\ z_1 e^{-ik_1 d_2} & -z_1^* e^{ik_1 d_2} \end{pmatrix}^{-1} \begin{pmatrix} \eta_1^+(-d_2) & \xi_1^+(-d_2) \\ \eta_1^-(-d_2) & \xi_1^-(-d_2) \end{pmatrix} \tag{28}$$

$$M_{23} = \begin{pmatrix} \eta_1^+(-d_1) & \xi_1^+(-d_1) \\ \eta_1^-(-d_1) & \xi_1^-(-d_1) \end{pmatrix}^{-1} \begin{pmatrix} \alpha e^{-ik_3 d_1} & \alpha e^{ik_3 d_1} \\ \beta z_3 e^{-ik_3 d_1} & -\beta z_3^* e^{ik_3 d_1} \end{pmatrix} \tag{29}$$

$$M_{34} = \begin{pmatrix} \alpha e^{ik_3 d_1} & \alpha e^{-ik_3 d_1} \\ \beta z_3 e^{ik_3 d_1} & -\beta z_3^* e^{-ik_3 d_1} \end{pmatrix}^{-1} \begin{pmatrix} \eta_{-1}^+(d_1) & \xi_{-1}^+(d_1) \\ \eta_{-1}^-(d_1) & \xi_{-1}^-(d_1) \end{pmatrix} \tag{30}$$

$$M_{45} = \begin{pmatrix} \eta_{-1}^+(d_2) & \xi_{-1}^+(d_2) \\ \eta_{-1}^-(d_2) & \xi_{-1}^-(d_2) \end{pmatrix}^{-1} \begin{pmatrix} e^{ik_1 d_2} & e^{-ik_1 d_2} \\ z_1 e^{ik_1 d_2} & -z_1^* e^{-ik_1 d_2} \end{pmatrix}. \tag{31}$$

These can be used to evaluate the reflection and transmission amplitudes

$$t_{s,n} = \frac{1}{m_{11}}, \qquad r_{s,n} = \frac{m_{21}}{m_{11}}. \tag{32}$$

Some symmetry relationship between the parabolic cylindric functions are worth mentioning. These are given by

$$\eta_{-1}^{\pm}(d_1) = \eta_1^{\pm}(-d_1), \qquad \eta_{-1}^{\pm}(d_2) = \eta_1^{\pm}(-d_2) \tag{33}$$

$$\xi_{-1}^{\pm}(d_1) = \xi_1^{\pm}(-d_1), \qquad \xi_{-1}^{\pm}(d_2) = \xi_1^{\pm}(-d_2). \tag{34}$$

We should point out at this stage that we were unfortunately forced to adopt a somehow cumbersome notation for our wavefunction parameters in different potential regions due to the relatively large number of necessary subscripts and superscripts. Before matching the eigenspinors at the boundaries, let us define the following shorthand notation

$$\eta_1^{\pm}(-d_1) = \eta_{11}^{\pm}, \qquad \eta_1^{\pm}(-d_2) = \eta_{12}^{\pm} \tag{35}$$

$$\xi_1^{\pm}(-d_1) = \xi_{11}^{\pm}, \qquad \xi_1^{\pm}(-d_2) = \xi_{12}^{\pm}. \tag{36}$$

At this level, we should determine the transmission amplitude $t_{s,n}$. After some lengthy algebra, one can solve the linear system given in (26) to obtain the transmission and reflection amplitudes in closed form. As far as the transmission is concerned, we find

$$t_{s,n} = \frac{\alpha\beta e^{2i(k_1 d_2 + k_3 d_1)} \left(1 + z_1^2\right) \left(1 + z_3^2\right)}{z_3 \left(e^{4ik_3 d_1} - 1\right) \left(\alpha^2 \mathcal{Y}_2 + \beta^2 \mathcal{Y}_1\right) + \alpha\beta \mathcal{Y}_3} \left(\xi_{11}^+ \eta_{11}^- - \xi_{11}^- \eta_{11}^+\right) \left(\xi_{12}^- \eta_{12}^+ - \xi_{12}^+ \eta_{12}^-\right) \tag{37}$$

where we have defined the following quantities

$$\mathcal{Y}_1 = \left(\xi_{12}^{-}\eta_{11}^{+} - \xi_{11}^{+}\eta_{12}^{-} - \xi_{12}^{+}\eta_{11}^{+}z_1 + \xi_{11}^{+}\eta_{12}^{+}z_1\right)\left(\xi_{11}^{+}\eta_{12}^{+} + \xi_{11}^{+}\eta_{12}^{-}z_1 - \eta_{11}^{+}(\xi_{12}^{+} + \xi_{12}^{-}z_1\right) \tag{38}$$

$$\mathcal{Y}_2 = \left(\xi_{11}^{-}\eta_{12}^{+} - \xi_{11}^{-}\eta_{12}^{-}z_1 - \eta_{11}^{-}(\xi_{12}^{+} + \xi_{12}^{+}z_1\right)\left(-\xi_{12}^{-}\eta_{11}^{-} + \xi_{12}^{+}\eta_{11}^{-}z_1 - \xi_{11}^{-}(\eta_{12}^{-} + \eta_{12}^{+}z_1\right) \tag{39}$$

$$\mathcal{Y}_3 = \Gamma_0\left(1 + z_1^2 z_3^2\right) + \Gamma_1 z_1\left(1 - z_3\right) + \Gamma_2\left(z_1^2 + z_3^2\right) + e^{4id_1k_3}\left(\Gamma_3 + \Gamma_4\right) \tag{40}$$

as well as

$$\begin{aligned}
\Gamma_0 &= -\xi_{12}^{+}\xi_{12}^{-}\eta_{11}^{+}\eta_{11}^{-} + \xi_{11}^{+}\xi_{12}^{-}\eta_{11}^{-}\eta_{12}^{+} + \xi_{11}^{-}\xi_{12}^{+}\eta_{11}^{+}\eta_{12}^{-} - \xi_{11}^{+}\xi_{11}^{-}\eta_{12}^{+}\eta_{12}^{-} && (41)\\
\Gamma_1 &= \left(\xi_{12}^{+}\right)^2\eta_{11}^{+}\eta_{11}^{-} - \left(\xi_{12}^{-}\right)^2\eta_{11}^{+}\eta_{11}^{-} - \xi_{11}^{-}\xi_{12}^{+}\eta_{11}^{+}\eta_{12}^{+} - \xi_{11}^{+}\xi_{12}^{+}\eta_{11}^{-}\eta_{12}^{+} && (42)\\
&\quad +\xi_{11}^{+}\xi_{11}^{-}\left(\eta_{12}^{+}\right)^2 - \xi_{11}^{+}\xi_{11}^{-}\left(\eta_{12}^{-}\right)^2 + \xi_{11}^{-}\xi_{12}^{-}\eta_{11}^{+}\eta_{12}^{-} + \xi_{11}^{+}\xi_{12}^{-}\eta_{11}^{-}\eta_{12}^{-} &&\\
\Gamma_2 &= \xi_{12}^{+}\xi_{12}^{-}\eta_{11}^{+}\eta_{11}^{-} - \xi_{11}^{-}\xi_{12}^{-}\eta_{11}^{+}\eta_{12}^{+} - \xi_{11}^{+}\xi_{12}^{+}\eta_{11}^{-}\eta_{12}^{-} + \xi_{11}^{+}\xi_{11}^{-}\eta_{12}^{+}\eta_{12}^{-} && (43)\\
\Gamma_3 &= \left(\xi_{12}^{+}\right)^2\eta_{11}^{+}\eta_{11}^{-}\left(z_3^2 - 1\right) - \xi_{11}^{-}\xi_{12}^{-}\eta_{11}^{+}\left[\eta_{12}^{+}\left(1 + z_1^2 z_3^2\right) - \eta_{12}^{-}z_1\left(z_3^2 - 1\right)\right] && (44)\\
&\quad +\xi_{11}^{-}\xi_{11}^{+}\left[\left(\eta_{12}^{+}\right)^2 z_1 - \left(\eta_{12}^{-}\right)^2 z_1 + \eta_{12}^{+}\eta_{12}^{-}\left(z_1^2 - 1\right)\left(z_3^2 - 1\right)\right] &&\\
\Gamma_4 &= \xi_{12}^{-}\eta_{11}^{-}\left[-\xi_{12}^{-}\eta_{11}^{+}z_1\left(z_3^2 - 1\right) + \xi_{11}^{+}\left(\eta_{12}^{-}z_0\left(z_3^2 - 1\right) + \eta_{12}^{+}\left(z_1^2 + z_3^2\right)\right)\right] && (45)\\
&\quad \xi_{12}^{+}\xi_{12}^{-}\eta_{11}^{+}\eta_{11}^{-}\left(z_1^2 + 1\right)\left(z_1^3 - 1\right) - \xi_{12}^{+}\xi_{11}^{+}\eta_{11}^{-}\left(\eta_{12}^{-}\left(1 + z_1^2 z_3^2\right) + \eta_{12}^{+}z_1\left(z_1^3 - 1\right)\right) &&\\
&\quad +\xi_{12}^{+}\xi_{11}^{-}\eta_{11}^{+}\left[\eta_{12}^{-}\left(z_1^2 + z_3^2\right) + \eta_{12}^{+}z_1\left(1 - z_3^2\right)\right]. &&
\end{aligned}$$

Now we are ready for the computation of the reflection $R_{s,n}$ and transmission $T_{s,n}$ coefficients. For this purpose, we introduce the associated current density J, which defines $R_{s,n}$ and $T_{s,n}$ as

$$T_{s,n} = \frac{J_{\mathsf{tra}}}{J_{\mathsf{inc}}}, \qquad R_{s,n} = \frac{J_{\mathsf{ref}}}{J_{\mathsf{inc}}} \tag{46}$$

where J_{inc}, J_{ref} and J_{tra} stand for the incident, reflected and transmitted components of the current density, respectively. It is easy to show that the current density J reads as

$$J = e\upsilon_F \Phi^{\dagger}\sigma_x\Phi \tag{47}$$

which gives the following results for the incident, reflected and transmitted components

$$J_{\mathsf{inc}} = e\upsilon_F(\Phi_1^{+})^{\dagger}\sigma_x\Phi_1^{+} \tag{48}$$

$$J_{\mathsf{ref}} = e\upsilon_F(\Phi_1^{-})^{\dagger}\sigma_x\Phi_1^{-} \tag{49}$$

$$J_{\mathsf{tra}} = e\upsilon_F\Phi_{\mathsf{5}}^{\dagger}\sigma_x\Phi_{\mathsf{5}}. \tag{50}$$

They allow us to express the transmission and reflection probabilities as

$$T_{s,n} = |t_{s,n}|^2, \qquad R_{s,n} = |r_{s,n}|^2. \tag{51}$$

The above results will be investigated numerically for different potential configurations to enable us to study the most important features of our system. Obviously, we can check that the probability conservation condition $T_{s,n} + R_{s,n} = 1$ is well satisfied. Let us consider Figure 2a) where we show the transmission and reflection probabilities versus the energy ϵ. In the first energy interval $\epsilon \leq k_y$ we have no transmission because it is a forbidden zone. However, for in second energy intervals $k_y \leq \epsilon \leq v_2 - k_y - \frac{\mu}{2}$ and $v_2 + k_y + \frac{\mu}{2} \leq \epsilon \leq v_1$, we observe resonance oscillations due to the Klein

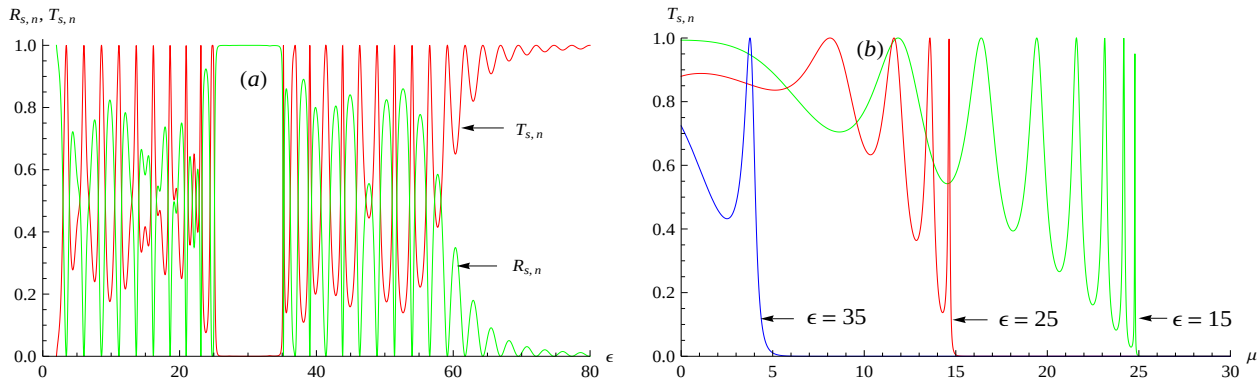

Figure 2: a) Transmission and reflection probabilities $(T_{s,n}, R_{s,n})$ as a function of energy ϵ with $d_1 = 0.6$, $d_2 = 2.5$, $\mu = 4$, $k_y = 2$, $v_1 = 60$ and $v_2 = 30$. b)Transmission probability $T_{s,n}$ as a function of energy gap μ with $d_1 = 0.5$, $d_2 = 1.5$, $\epsilon = \{15, 25, 35\}$, $k_y = 1$, $v_1 = 50$ and $v_2 = 40$.

regime. We have no transmission (like a windows) when $v_2 - k_y - \frac{\mu}{2} \leq \epsilon \leq v_2 + k_y + \frac{\mu}{2}$. Finally in the interval where $\epsilon > v_1$, there exist usual high energy oscillations, which asymptotically saturates at high energy. Note that (18) implies that for certain energy gap μ, there is no transmission. In fact, under the condition

$$\mu > |v_2 - \epsilon| \tag{52}$$

every incoming wave is reflected. In Figure 2b) we see that the transmission vanishes for values of ϵ below the critical value $\mu = |v_2 - \epsilon|$.

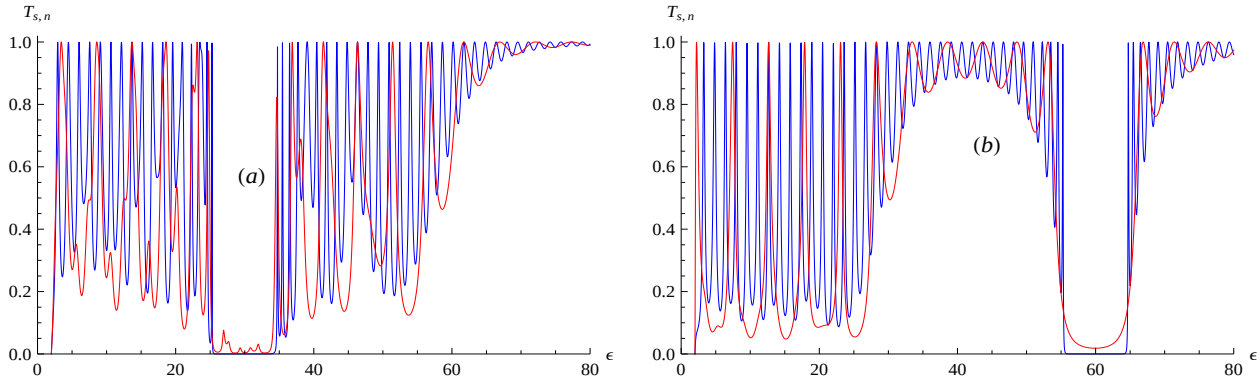

Figure 3: (Color online) Transmission probability for the static barrier $T_{s,n}$ as a function of energy ϵ with $d_1 = 0.3$ color red, $d_1 = 1$, $d_2 = 2.5$, $\mu = 4$ and $k_y = 2$. a) the parameters: $v_1 = 60$, $v_2 = 30$. b) $v_1 = 30$, $v_2 = 60$.

Figure 3 presents the transmission $T_{s,n}$ as a function of incident electron energy ϵ for the Dirac fermion scattered by a double triangular barriers with $d_2 = 2.5$, $\mu = 4$, $k_y = 2$ and two values of barrier height $d_1 = \{0.3, 1\}$. We consider in Figure 3a) the parameters: $v_1 = 2v_2 = 60$, the results show that as long as the well width d_1 increases the transmission resonance shifts and the width of the resonances increases between $k_y \leq \epsilon \leq v_2 - k_y - \frac{\mu}{2}$ and $v_2 + k_y + \frac{\mu}{2} \leq \epsilon \leq v_1$. In Figure 3b) we consider the parameters $v_1 = \frac{v_2}{2} = 30$ for the Dirac fermion scattered by a double barrier triangular

potential where we distinguish five different zones.

- The first is a forbidden zone where $0 \leq \epsilon \leq k_y$.
- The second zone $k_y \leq \epsilon \leq v_1$ is the upper Klein energy zone with transmission resonances.
- The third zone contains oscillations.
- The fourth one $v_2 - k_y - \frac{\mu}{2} \leq \epsilon \leq v_2 + k_y + \frac{\mu}{2}$ is a window where the transmission is zero, the wavefunction is damped and transmission decays exponentially.
- The fifth zone $\epsilon \geq v_2 + k_y + \frac{\mu}{2}$ contains oscillations, the transmission converges to unity at high energies similarly to the non-relativistic result.

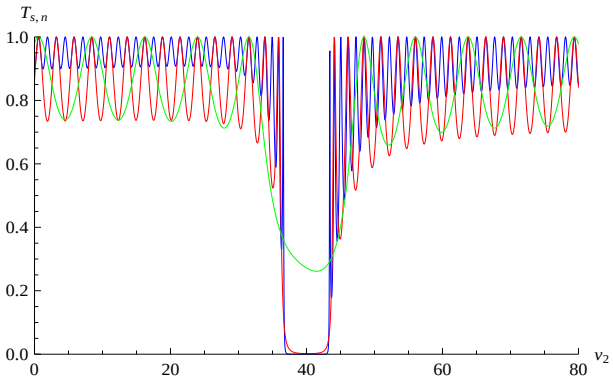

Figure 4: (Color online) Transmission probability for the static barrier $T_{s,n}$ as a function of energy potential v_2 with $d_1 = 0.2$ color red, $d_1 = 0.6$ color green, $d_1 = 1.2$ color blue, $d_2 = 2$, $\mu = 3$, $k_y = 1$, $\epsilon = 40$ and $v_1 = 60$.

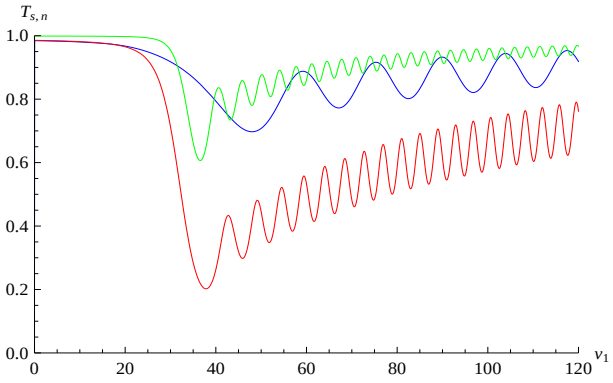

Figure 5: (Color online) Transmission probability for the static barrier $T_{s,n}$ as a function of energy potential v_1 with $d_1 = 0.7$ color red, $d_1 = 2$ color blue, $d_1 = 0.05$ color green, $d_2 = 2.5$, $\mu = 4$, $k_y = 2$, $\epsilon = 30$ and $v_2 = 60$. .

We represent in Figure 4 the transmission versus potential energy v_2. It is clear that the two transmission curves are symmetric with respect to the point $v_2 = \epsilon$. While an increase in the value d_1 widens the bowl width. Figure 5 presents the transmission probability for a static barrier $T_{s,n}$ as

function of the strength of the applied voltage v_1. The transmission is observed for small values of v_1 less than the energy of the incident fermion. It then decreases sharply for $v_1 > \epsilon - (2k_y + \mu)$ until it reaches a relative minimum and then begins to increase in an oscillatory manner.

4 Magnetic double barrier

Consider a two-dimensional system of Dirac fermions forming a graphene sheet. This sheet is subject to a double barrier potential in addition to a mass term and an externally applied magnetic field as shown in Figure 6. Particles and antiparticles moving respectively in the positive and negative energy regions with the tangential component of the wave vector along the x-direction have translation invariance in the y-direction. A uniform perpendicular magnetic field is applied, along the z-direction and confined to the well region between the two barriers. It is defined by

$$B(x, y) = B\Theta(d_1^2 - x^2) \tag{53}$$

where B is the strength of the magnetic field within the strip located in the region $|x| < d_1$ and $B = 0$ otherwise, Θ is the Heaviside step function. Choosing the Landau gauge and imposing continuity of the vector potential at the boundary to avoid unphysical effects, we end up with the following vector potential

$$A_y(x) = A_j = \frac{c}{e} \times \begin{cases} -\frac{1}{l_B^2} d_1, & x < -d_2 \\ \frac{1}{l_B^2} x, & \mid x \mid < d_1 \\ \frac{1}{l_B^2} d_1, & x \geq d_2 \end{cases} \tag{54}$$

with the magnetic length is $l_B = \sqrt{1/B}$ in the unit system ($\hbar = c = e = 1$). The system contains

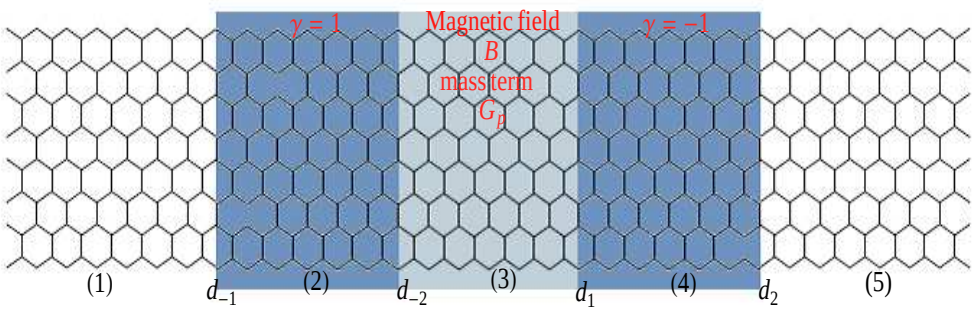

Figure 6: Schematic diagram for the monolayer graphene double barrier.

five regions denoted $\mathsf{j} = 1, 2, 3, 4, 5$. The left region ($\mathsf{j} = 1$) describes the incident electron beam with the energy $E = v_F\epsilon$ at an incident angle ϕ_1 where v_F is the Fermi velocity. The extreme right region ($\mathsf{j} = 5$) describes the transmitted electron beam at an angle ϕ_5. The Hamiltonian for one-pseudospin component describing our system reads as

$$H_m = v_F \boldsymbol{\sigma} \cdot \left(\mathbf{p} + \frac{e}{c} \mathbf{A} \right) + V(x)\mathbb{I}_2 + G_p \Theta \left(d_1^2 - x^2 \right) \sigma_z \tag{55}$$

To proceed further, we need to find the solutions of the corresponding Dirac equation and their associated energy spectrum.

4.1 Energy spectrum solutions

We are set to determine the eigenvalues and eigenspinors of the Hamiltonian H_m. Indeed, the Dirac Hamiltonian describing regions 1 and 5, is obtained from (55) as

$$H_m = \begin{pmatrix} 0 & \upsilon_F \left(p_{x\mathrm{j}} - i\left(p_y + \frac{e}{c}A_{\mathrm{j}}\right)\right) \\ \upsilon_F \left(p_{x\mathrm{j}} + i\left(p_y + \frac{e}{c}A_{\mathrm{j}}\right)\right) & 0 \end{pmatrix}. \tag{56}$$

The corresponding time independent Dirac equation for the spinor $\psi_{\mathrm{j}}(x,y) = (\varphi_{\mathrm{j}}^{+}, \varphi_{\mathrm{j}}^{-})^T$ at energy $E = \upsilon_F \epsilon$ is given by

$$H_m \begin{pmatrix} \varphi_{\mathrm{j}}^{+} \\ \varphi_{\mathrm{j}}^{-} \end{pmatrix} = \epsilon \begin{pmatrix} \varphi_{\mathrm{j}}^{+} \\ \varphi_{\mathrm{j}}^{-} \end{pmatrix}. \tag{57}$$

This eigenproblem can be written as two linear differential equations of the from

$$p_{x\mathrm{j}} - i\left(p_y + \frac{e}{c}A_{\mathrm{j}}\right)\varphi_{\mathrm{j}}^{-} = \epsilon\varphi_{\mathrm{j}}^{+} \tag{58}$$

$$p_{x\mathrm{j}} + i\left(p_y + \frac{e}{c}A_{\mathrm{j}}\right)\varphi_{\mathrm{j}}^{+} = \epsilon\varphi_{\mathrm{j}}^{-} \tag{59}$$

which gives the energy eigenvalue

$$\epsilon = s_{\mathrm{j}}\sqrt{p_{x\mathrm{j}}^2 + \left(p_y + \frac{e}{c}A_{\mathrm{j}}\right)} \tag{60}$$

where $s_{\mathrm{j}} = \mathrm{sign}(\epsilon)$. This implies

$$p_{x\mathrm{j}} = \sqrt{\epsilon^2 - \left(p_y + \frac{e}{c}A_{\mathrm{j}}\right)^2} \tag{61}$$

with incoming momentum $\boldsymbol{p_{\mathrm{j}}} = (p_{x\mathrm{j}}, p_y)$ and $\boldsymbol{r} = (x,y)$. The incoming wave function is

$$\psi_{in} = \frac{1}{\sqrt{2}} \begin{pmatrix} 1 \\ z_{p_{x\mathrm{j}}} \end{pmatrix} e^{\boldsymbol{i}\boldsymbol{p_{\mathrm{j}}}\boldsymbol{r}} \tag{62}$$

$$z_{p_{x\mathrm{j}}} = z_{\mathrm{j}} = s_{\mathrm{j}} \frac{p_{x\mathrm{j}} + i(p_y + \frac{e}{c}A_{\mathrm{j}})}{\sqrt{(p_{x\mathrm{j}})^2 + (p_y + \frac{e}{c}A_{\mathrm{j}})^2}} = s_{\mathrm{j}} e^{i\phi_{\mathrm{j}}} \tag{63}$$

where $s_0 = \mathrm{sgn}(\epsilon)$ and $\phi_{\mathrm{j}} = \arctan\left(\frac{p_y - \frac{e}{c}A_{\mathrm{j}}}{p_{x\mathrm{j}}}\right)$ is the angle that the incident electrons make with the x-direction, p_{x1} and p_y are the x and y-components of the electron wave vector, respectively. The eigenspinors are given by

$$\psi_{\mathrm{j}}^{+} = \frac{1}{\sqrt{2}} \begin{pmatrix} 1 \\ z_{\mathrm{j}} \end{pmatrix} e^{\boldsymbol{i}(p_{x\mathrm{j}}x + p_y y)} \tag{64}$$

$$\psi_{\mathrm{j}}^{-} = \frac{1}{\sqrt{2}} \begin{pmatrix} 1 \\ -z_{\mathrm{j}}^{*} \end{pmatrix} e^{\boldsymbol{i}(-p_{x\mathrm{j}}x + p_y y)}. \tag{65}$$

It is straightforward to solve the tunneling problem for Dirac fermions. We assume that the incident wave propagates at the angle ϕ_1 with respect to the x-direction and write the components, of the Dirac spinor φ_{j}^{+} and φ_{j}^{-}, for each region, in the following form

⋆ For $x < -d_2$ (region 1):

$$\epsilon = \left[p_{x1}^2 + \left(p_y - \frac{1}{l_B^2}d_1\right)^2\right]^{\frac{1}{2}} \tag{66}$$

$$\psi_1 = \frac{1}{\sqrt{2}}\begin{pmatrix} 1 \\ z_1 \end{pmatrix} e^{\boldsymbol{i}(p_{x1}x+p_y y)} + r_m \frac{1}{\sqrt{2}}\begin{pmatrix} 1 \\ -z_1^* \end{pmatrix} e^{\boldsymbol{i}(-p_{1x}x+p_y y)} \tag{67}$$

$$z_1 = s_1 \frac{p_{x1} + i\left[p_y - \frac{1}{l_B^2}d_1\right]}{\sqrt{p_{x1}^2 + \left[p_y - \frac{1}{l_B^2}d_1\right]^2}}. \tag{68}$$

⋆ In the barrier $x > d_2$ (region 5)

$$\epsilon = \left[p_{x5}^2 + \left(p_y + \frac{1}{l_B^2}d_1\right)^2\right]^{\frac{1}{2}} \tag{69}$$

$$\psi_5 = \frac{1}{\sqrt{2}}t_m \begin{pmatrix} 1 \\ z_5 \end{pmatrix} e^{\boldsymbol{i}(p_{x5}x+p_y y)} \tag{70}$$

$$z_5 = s_5 \frac{p_{x5} + i\left[p_y + \frac{1}{l_B^2}d_1\right]}{\sqrt{p_{x1}^2 + \left[p_y + \frac{1}{l_B^2}d_1\right]^2}}. \tag{71}$$

⋆ In region 2 and 4 ($d_1 < |x| < d_2$): The general solution can be expressed in terms of the parabolic cylinder function [14, 19, 20] as

$$\chi_\gamma^+ = c_1 D_{\nu_\gamma - 1}\left(Q_\gamma\right) + c_2 D_{-\nu_\gamma}\left(-Q_\gamma^*\right) \tag{72}$$

where $\nu_\gamma = \frac{i}{2\varrho}\left(k_y - \gamma\frac{d_1}{l_B^2}\right)^2$, $\epsilon_0 = \epsilon - v_1$ and $Q_\gamma(x) = \sqrt{\frac{2}{\varrho}}e^{i\pi/4}\left(\gamma\varrho x + \epsilon_0\right)$, c_1 and c_2 are constants and gives the other component

$$\begin{aligned}\chi_\gamma^- &= -c_2\frac{1}{k_y - \gamma\frac{d_1}{l_B^2}}\left[2(\epsilon_0 + \gamma\varrho x)D_{-\nu_\gamma}\left(-Q_\gamma^*\right) + \sqrt{2\varrho}e^{i\pi/4}D_{-\nu_\gamma+1}\left(-Q_\gamma^*\right)\right] \\ &\quad -\frac{c_1}{k_y - \gamma\frac{d_1}{l_B^2}}\sqrt{2\varrho}e^{-i\pi/4}D_{\nu_\gamma-1}\left(Q_\gamma\right)\end{aligned} \tag{73}$$

The components of the spinor solution of the Dirac equation (4) in region 2 and 4 can be obtained from (72) and (73) with $\varphi_\gamma^+(x) = \chi_\gamma^+ + i\chi_\gamma^-$ and $\varphi_\gamma^-(x) = \chi_\gamma^+ - i\chi_\gamma^-$. We have the eigenspinor

$$\psi_{\mathsf{j}} = a_{\mathsf{j}-1}\begin{pmatrix} u_\gamma^+(x) \\ u_\gamma^-(x) \end{pmatrix} e^{ik_y y} + a_{\mathsf{j}}\begin{pmatrix} v_\gamma^+(x) \\ v_\gamma^-(x) \end{pmatrix} e^{ik_y y} \tag{74}$$

where $\mathsf{j} = 2, 4$ and $\gamma = \pm 1$, the function $u_\gamma^\pm(x)$ and $v_\gamma^\pm(x)$ are given by

$$u_\gamma^\pm(x) = D_{\nu_\gamma-1}\left(Q_\gamma\right) \mp \frac{1}{k_y - \gamma\frac{d_1}{l_B^2}}\sqrt{2\varrho}e^{i\pi/4}D_{\nu_\gamma}\left(Q_\gamma\right) \tag{75}$$

$$\begin{aligned}v_\gamma^\pm(x) &= \pm\frac{1}{k_y - \gamma\frac{d_1}{l_B^2}}\sqrt{2\varrho}e^{-i\pi/4}D_{-\nu_\gamma+1}\left(-Q_\gamma^*\right) \\ &\quad \pm\frac{1}{k_y - \gamma\frac{d_1}{l_B^2}}\left(-2i\epsilon_0 \pm \left(k_y - \gamma\frac{d_1}{l_B^2}\right) - \gamma 2i\varrho x\right)D_{-\nu_\gamma}\left(-Q_\gamma^*\right).\end{aligned} \tag{76}$$

In region 2:

$$\psi_2 \;=\; a_1 \begin{pmatrix} u_1^+(x) \\ u_1^-(x) \end{pmatrix} e^{ik_y y} + a_2 \begin{pmatrix} v_1^+(x) \\ v_1^-(x) \end{pmatrix} e^{ik_y y} \tag{77}$$

In region 4:

$$\psi_4 \;=\; a_3 \begin{pmatrix} u_{-1}^+(x) \\ u_{-1}^-(x) \end{pmatrix} e^{ik_y y} + a_4 \begin{pmatrix} v_{-1}^+(x) \\ v_{-1}^-(x) \end{pmatrix} e^{ik_y y} \tag{78}$$

$\star$ In the region $|x| \leq d_1$: From the nature of the system under consideration, we write the Hamiltonian corresponding to region 3 in matrix form as

$$H_m = v_F \begin{pmatrix} \frac{V_2}{v_F} + \frac{G_p}{v_F} & -i\frac{\sqrt{2}}{l_B}\left(\frac{l_B}{\sqrt{2}}\left(\partial_x - i\partial_y + \frac{e}{c}A_3\right)\right) \\ i\frac{\sqrt{2}}{l_B}\left(\frac{l_B}{\sqrt{2}}\left(-\partial_x - i\partial_y + \frac{e}{c}A_3\right)\right) & \frac{V_2}{v_F} - \frac{G_p}{v_F} \end{pmatrix} \tag{79}$$

Note that, the energy gap G_p behaves like a mass term in Dirac equation. Certainly this will affect the above results and lead to interesting consequences on the transport properties of our system. We determine the eigenvalues and eigenspinors of the Hamiltonian H_m by considering the time independent equation for the spinor $\psi_3(x,y) = (\psi_3^+, \psi_3^-)^T$ using the fact that the transverse momentum p_y is conserved, we can write the wave function $\psi_3(x,y) = e^{ip_y y}\varphi_3(x)$ with $\varphi_3(x) = (\varphi_3^+, \varphi_3^-)^T$, the energy being defined by $E = \upsilon_F \epsilon$ leads to

$$H_m \begin{pmatrix} \varphi_3^+ \\ \varphi_3^- \end{pmatrix} = \epsilon \begin{pmatrix} \varphi_3^+ \\ \varphi_3^- \end{pmatrix} \tag{80}$$

At this stage, it is convenient to introduce the annihilation and creation operators. They can be defined as

$$a = \frac{l_B}{\sqrt{2}}\left(\partial_x + k_y + \frac{e}{c}A_3\right), \qquad a^\dagger = \frac{l_B}{\sqrt{2}}\left(-\partial_x + k_y + \frac{e}{c}A_3\right) \tag{81}$$

which obey the canonical commutation relations $[a, a^\dagger] = \mathbb{I}$. Rescaling our energies $G_p = \upsilon_F \mu$ and $V_2 = \upsilon_F v_2$, (80) can be written in terms of a and $a^\dagger$ as

$$\begin{pmatrix} v_2 + \mu & -i\frac{\sqrt{2}}{l_B}a \\ +i\frac{\sqrt{2}}{l_B}a^\dagger & v_2 - \mu \end{pmatrix} \begin{pmatrix} \varphi_3^+ \\ \varphi_3^- \end{pmatrix} = \epsilon \begin{pmatrix} \varphi_3^+ \\ \varphi_3^- \end{pmatrix} \tag{82}$$

which gives

$$(v_2 + \mu)\varphi_3^+ - i\frac{\sqrt{2}}{l_B}a\varphi_3^- = \epsilon\varphi_3^+ \tag{83}$$

$$i\frac{\sqrt{2}}{l_B}a^\dagger\varphi_3^+ + (v_2 - \mu)\varphi_3^- = \epsilon\varphi_3^-. \tag{84}$$

Injecting (84) in (83), we obtain a differential equation of second order for φ_3^+

$$\left[(\epsilon - v_2)^2 - \mu^2\right]\varphi_3^+ = \frac{2}{l_B^2}aa^\dagger\varphi_3^+. \tag{85}$$

It is clear that φ_3^+ is an eigenstate of the number operator $\widehat{N} = a^\dagger a$ and therefore we identify φ_3^+ with the eigenstates of the harmonic oscillator $|n-1\rangle$, namely

$$\varphi_3^+ \sim | \, n-1\rangle \tag{86}$$

which is equivalent to

$$\left[(\epsilon - v_2)^2 - \mu^2\right] \mid n-1\rangle = \frac{2}{l_B^2} n \mid n-1\rangle \tag{87}$$

and the associated energy spectrum is

$$\epsilon - v_2 = s_3 \epsilon_n = s_3 \frac{1}{l_B} \sqrt{(\mu l_B)^2 + 2n} \tag{88}$$

where we have set $\epsilon_n = s_3(\epsilon - v_2)$ and $s_3 = \text{sign}(\epsilon_n - v_2)$ correspond to positive and negative energy solutions. For this reason we write the eigenvalues as

$$\epsilon = v_2 + s_3 \frac{1}{l_B} \sqrt{(\mu l_B)^2 + 2n} \tag{89}$$

The second eigenspinor component then can be obtained from

$$\varphi_3^- = \frac{i\sqrt{2}a^\dagger}{(\epsilon - v_2) l_B + \mu l_B} \mid n-1\rangle = \frac{i\sqrt{2n}}{(\epsilon - v_2) l_B + \mu l_B} \mid n\rangle \tag{90}$$

where $\sqrt{2n} = \sqrt{(\epsilon_n l_B)^2 - (\mu l_B)^2}$. We find

$$\varphi_3^- = s_3 i \sqrt{\frac{\epsilon_n l_B - s_3 \mu l_B}{\epsilon_n l_B + s_3 \mu l_B}} \mid n\rangle \tag{91}$$

After normalization we arrive at the following expression for the positive and negative energy eigenstates

$$\varphi_3 = \frac{1}{\sqrt{2}} \begin{pmatrix} \sqrt{\frac{\epsilon_n l_B + s_3 \mu l_B}{\epsilon_n l_B}} \mid n-1\rangle \\ s_3 i \sqrt{\frac{\epsilon_n l_B - s_3 \mu l_B}{\epsilon_n l_B}} \mid n\rangle \end{pmatrix} \tag{92}$$

Introducing the parabolic cylinder functions $D_n(x) = 2^{-\frac{n}{2}} e^{-\frac{x^2}{4}} H_n\left(\frac{x}{\sqrt{2}}\right)$ to express the solution in region 3 as

$$\psi_3(x,y) = b_1 \psi_3^+ + b_2 \psi_3^- \tag{93}$$

with the two components

$$\psi_3^\pm(x,y) = \frac{1}{\sqrt{2}} \begin{pmatrix} \sqrt{\frac{\epsilon_n l_B + s_3 \mu l_B}{\epsilon_n l_B}} D_{(\epsilon_n l_B)^2 - (\mu l_B)^2)/2 - 1}\left(\pm\sqrt{2}\left(\frac{x}{l_B} + k_y l_B\right)\right) \\ \pm i \frac{s_3\sqrt{2}}{\sqrt{\epsilon_n l_B (\epsilon_n l_B + s_3 \mu l_B)}} D_{(\epsilon_n l_B)^2 - (\mu l_B)^2)/2}\left(\pm\sqrt{2}\left(\frac{x}{l_B} + k_y l_B\right)\right) \end{pmatrix} e^{i k_y y} \tag{94}$$

As usual the coefficients $(a_1, a_2, a_3, a_4, b_1, b_2, r, t)$ can be determined using the boundary conditions, continuity of the eigenspinors at each interface.

4.2 Transmission and reflection amplitudes

We will now study some interesting features of our system in terms of the corresponding transmission probability. Before doing so, let us simplify our writing using the following shorthand notation

$$\vartheta_{\tau 1}^{\pm} = D_{[(\epsilon_n l_B)^2-(\mu l_B)^2]/2-1}\left[\pm\sqrt{2}\left(\frac{\tau d_1}{l_B}+k_y l_B\right)\right] \tag{95}$$

$$\zeta_{\tau 1}^{\pm} = D_{[(\epsilon_n l_B)^2-(\mu l_B)^2]/2}\left[\pm\sqrt{2}\left(\frac{\tau d_1}{l_B}+k_y l_B\right)\right] \tag{96}$$

$$f_1^{\pm} = \sqrt{\frac{\epsilon_n \pm \mu}{\epsilon_n}}, \qquad f_2^{\pm} = \frac{\sqrt{2/l_B^2}}{\sqrt{\epsilon_n(\epsilon_n \pm \mu)}} \tag{97}$$

$$u_\gamma^{\pm}(\tau d_1) = u_{\gamma,\tau 1}^{\pm}, \qquad u_\gamma^{\pm}(\tau d_2) = u_{\gamma,\tau 2}^{\pm} \tag{98}$$

$$v_\gamma^{\pm}(\tau d_1) = v_{\gamma,\tau 1}^{\pm}, \qquad v_\gamma^{\pm}(\tau d_2) = v_{\gamma,\tau 2}^{\pm} \tag{99}$$

where $\tau = \pm$. Dirac equation requires the following set of continuity equations

$$\psi_1(-d_2) = \psi_2(-d_2) \tag{100}$$

$$\psi_2(-d_1) = \psi_3(-d_1) \tag{101}$$

$$\psi_3(d_1) = \psi_4(d_1) \tag{102}$$

$$\psi_4(d_2) = \psi_5(d_2) \tag{103}$$

That is requiring the continuity of the spinor wave functions at each junction interface give rise to the above set of equations. We prefer to express these relationships in terms of 2×2 transfer matrices between j-th and j+1-th regions, $\mathcal{M}_{\mathrm{j,j+1}}$, we obtain the full transfer matrix over the whole double barrier which can be written, in an obvious notation, as follows

$$\begin{pmatrix} 1 \\ r_m \end{pmatrix} = \prod_{\mathrm{j}=1}^{4} \mathcal{M}_{\mathrm{j,j+1}} \begin{pmatrix} t_m \\ 0 \end{pmatrix} = \mathcal{M} \begin{pmatrix} t_m \\ 0 \end{pmatrix} \tag{104}$$

where the total transfer matrix $\mathcal{M} = \mathcal{M}_{12}\cdot\mathcal{M}_{23}\cdot\mathcal{M}_{34}\cdot\mathcal{M}_{45}$ are transfer matrices that couple the wave function in the j-th region to the wave function in the $\mathrm{j}+1$-th region. These are given explicitly by

$$\mathcal{M} = \begin{pmatrix} \tilde{m}_{11} & \tilde{m}_{12} \\ \tilde{m}_{21} & \tilde{m}_{22} \end{pmatrix} \tag{105}$$

$$\mathcal{M}_{12} = \begin{pmatrix} e^{-ip_{x1}d_2} & e^{ip_{x1}d_2} \\ z_1 e^{-ip_{x1}d_2} & -z_1^* e^{ip_{x1}d_2} \end{pmatrix}^{-1} \begin{pmatrix} u_{1,-2}^{+} & v_{1,-2}^{+} \\ u_{1,-2}^{-} & v_{1,-2}^{-} \end{pmatrix} \tag{106}$$

$$\mathcal{M}_{23} = \begin{pmatrix} u_{1,-1}^{+} & v_{1,-1}^{+} \\ u_{1,-1}^{-} & v_{1,-1}^{-} \end{pmatrix}^{-1} \begin{pmatrix} \vartheta_1^{+} & \vartheta_1^{-} \\ \zeta_1^{+} & \zeta_1^{-} \end{pmatrix} \tag{107}$$

$$\mathcal{M}_{34} = \begin{pmatrix} \vartheta_{-1}^{+} & \vartheta_{-1}^{-} \\ \zeta_{-1}^{+} & \zeta_{-1}^{-} \end{pmatrix}^{-1} \begin{pmatrix} u_{-1,1}^{+} & v_{-1,1}^{+} \\ u_{-1,1}^{-} & v_{-1,1}^{-} \end{pmatrix} \tag{108}$$

$$\mathcal{M}_{45} = \begin{pmatrix} u_{-1,2}^{+} & v_{-1,2}^{+} \\ u_{-1,2}^{-} & v_{-1,2}^{-} \end{pmatrix}^{-1} \begin{pmatrix} e^{ip_{x5}d_2} & e^{-ip_{x5}d_2} \\ z_5 e^{ip_{x5}d_2} & -z_5^* e^{-ip_{x5}d_2} \end{pmatrix}. \tag{109}$$

These will enable us to compute the reflection and transmission amplitudes

$$t_m = \frac{1}{\tilde{m}_{11}}, \qquad r_m = \frac{\tilde{m}_{21}}{\tilde{m}_{11}}. \tag{110}$$

More explicitly, we have for transmission

$$t_m = \frac{e^{id_2(p_{x1}+p_{x5})}\left(1+z_5^2\right)\left(\vartheta_1^-\zeta_1^+ + \vartheta_1^+\zeta_1^-\right)}{f_2^+\left(f_1^-\mathcal{L}_1 + if_2^-\mathcal{L}_2\right) + f_1^+\left(f_2^-\mathcal{L}_3 + if_1^-\mathcal{L}_4\right)}\mathcal{D} \tag{111}$$

where the quantities $\mathcal{D}$, $\mathcal{L}_1$, $\mathcal{L}_2$, $\mathcal{L}_3$ and $\mathcal{L}_4$ are defined by

$$\begin{aligned}
\mathcal{D} &= \left(u_{-1,1}^- v_{-1,1}^+ - u_{-1,1}^+ v_{-1,1}^-\right)\left(u_{1,-2}^+ v_{1,-2}^- - u_{1,-2}^- v_{1,-2}^+\right) && (112)\\
\mathcal{L}_1 &= \vartheta_{-1}^-\zeta_1^+\mathcal{F}\mathcal{G} - \vartheta_1^-\zeta_{-1}^+\mathcal{K}\mathcal{J} && (113)\\
\mathcal{L}_2 &= \left(\zeta_1^+\zeta_{-1}^- - \zeta_1^-\zeta_{-1}^+\right)\mathcal{F}\mathcal{J} && (114)\\
\mathcal{L}_3 &= \vartheta_{-1}^+\zeta_1^-\mathcal{F}\mathcal{G} - \vartheta_1^+\zeta_{-1}^-\mathcal{K}\mathcal{J} && (115)\\
\mathcal{L}_4 &= = \left(\vartheta_1^+\vartheta_{-1}^- - \vartheta_1^-\vartheta_{-1}^+\right)\mathcal{K}\mathcal{G} && (116)
\end{aligned}$$

and

$$\begin{aligned}
\mathcal{F} &= \left[u_{1,-1}^+ v_{1,-2}^- - u_{1,-2}^- v_{1,-1}^+ - z_1\left(u_{1,-1}^+ v_{1,-2}^+ - u_{1,-2}^+ v_{1,-1}^+\right)\right] && (117)\\
\mathcal{G} &= \left[u_{-1,1}^- v_{-1,2}^+ - u_{-1,2}^+ v_{-1,1}^- + z_5\left(u_{-1,1}^- v_{-1,2}^- - u_{-1,2}^- v_{-1,1}^-\right)\right] && (118)\\
\mathcal{K} &= \left[u_{1,-1}^- v_{1,-2}^- - u_{1,-2}^- v_{1,-1}^- - z_1\left(u_{1,-1}^- v_{1,-2}^+ - u_{1,-2}^+ v_{1,-1}^-\right)\right] && (119)\\
\mathcal{J} &= \left[u_{-1,1}^+ v_{-1,2}^+ - u_{-1,2}^+ v_{-1,1}^+ + z_5\left(u_{-1,1}^+ v_{-1,2}^- - u_{-1,2}^- v_{-1,1}^+\right)\right] && (120)
\end{aligned}$$

Actually what we need are exactly the transmission T_m and reflection R_m probabilities. These can be obtained using the electric current density J corresponding to our system. From our previous Hamiltonian, we can show incident, reflected and transmitted current take the form

$$\begin{aligned}
J_{\mathsf{inc,m}} &= e\upsilon_F(\psi_1^+)^\dagger\sigma_x\psi_1^+ && (121)\\
J_{\mathsf{ref,m}} &= e\upsilon_F(\psi_1^-)^\dagger\sigma_x\psi_1^- && (122)\\
J_{\mathsf{tra,m}} &= e\upsilon_F\psi_5^\dagger\sigma_x\psi_5. && (123)
\end{aligned}$$

These can be used to write the reflection and transmission probabilities as

$$T_m = \frac{p_{x5}}{p_{x1}}|t_m|^2, \qquad R_m = |r_m|^2. \tag{124}$$

The physical outcome of particle scattering through the double triangular barrier depends on the energy of the incoming particle. We numerically evaluate the transmission probability T_m as a function of structural parameters of the graphene double triangular barrier with a perpendicular magnetic field, including the energy ϵ, the y-component of the wave vector k_y, the magnetic field B, the energy gap μ and the applied potentials v_1 and v_2. The results are shown in Figures 7, 8 and 9. In addition to the expected above-barrier full transmission for some values of ϵl_B and $v_2 l_B$.

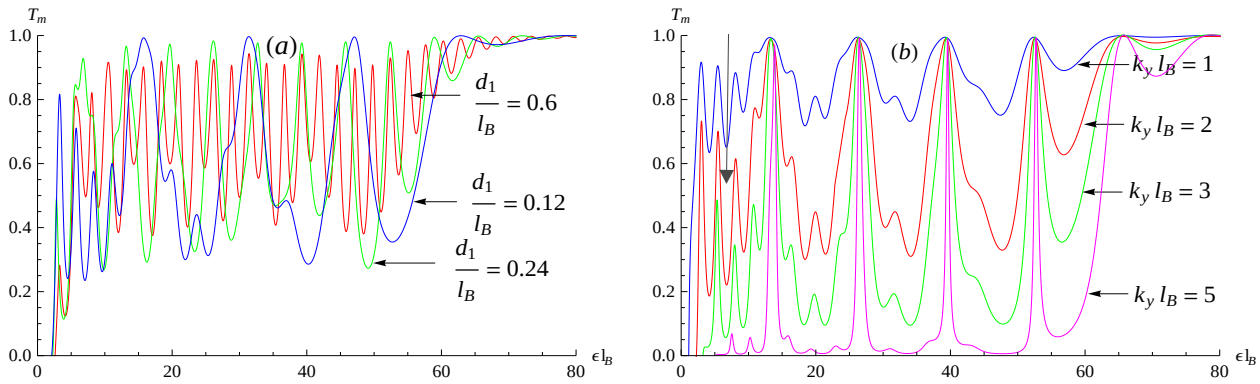

Figure 7: (Color online) Transmission probability T_m for the magnetic barrier as a function of energy ϵl_B with $\frac{d_2}{l_B} = 1.5$, $v_1 l_B = 60$, $v_2 l_B = 0$ and $\mu l_B = 0$. (a) the parameters: $k_y l_B = 2$ and $\frac{d_1}{l_B} = \{0.12, 0.24, 0.6\}$. (b) the parameters: $\frac{d_1}{l_B} = 0.12$ and $k_y l_B = \{1, 2, 3, 5\}$

We note that in Figure 7a), when the energy is less than the height of the potential barrier $\epsilon l_B < k_y l_B + \frac{d_1}{l_B}$, we have zero transmission. In the second interval $k_y l_B + \frac{d_1}{l_B} \leq \epsilon l_B \leq v_1 l_B$ the third zone contains oscillations. Finally the interval $\epsilon l_B > v_1 l_B$ contains the usual high energy barrier oscillations and asymptotically goes to unity at high energy. Figure 7b) shows the transmission spectrum for different wave vector $k_y l_B$, the energy gap μl_B is zero and $v_2 l_B = 0$. We see that if we increase the wave vector $k_y l_B$ the zone of zero transmission increases following the condition $\epsilon l_B < k_y l_B + \frac{d_1}{l_B}$. In the second interval the transmission oscillates between the value of the total transmission and zero as $k_y l_B$ increases. Finally in the interval $\epsilon l_B > v_1 l_B$ the transmission increases.

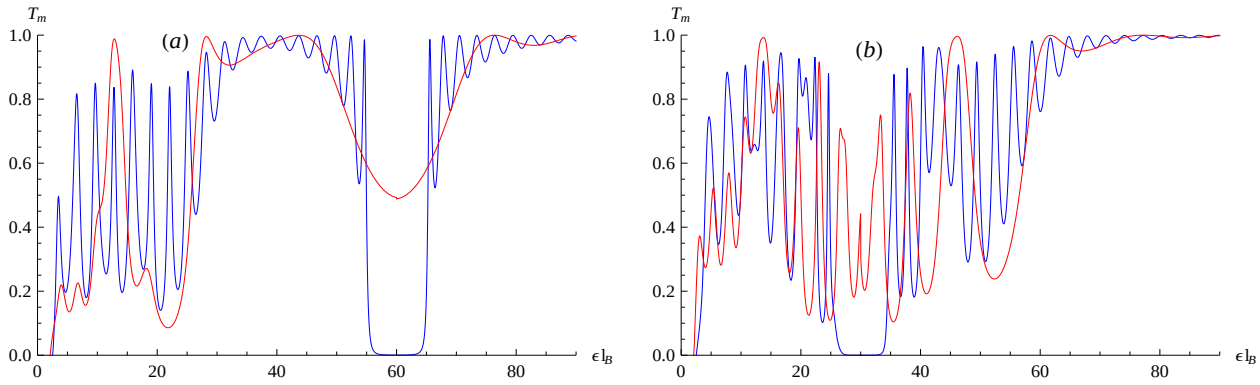

Figure 8: (Color online) Transmission probability T_m for the magnetic barrier as a function of energy E with $\frac{d_1}{l_B} = 0.1$ color red, $\frac{d_1}{l_B} = 0.5$ color blue, $\frac{d_2}{l_B} = 1.5$, $\mu l_B = 4$ and $k_y l_B = 2$. a) the parameters: $v_1 l_B = 30$, $v_2 l_B = 60$. b) the parameters: $v_1 l_B = 60$, $v_2 l_B = 30$.

On the other hand, if we keep the same well region and cancel both the applied magnetic field and mass term in the well region, the series of potentials behave like a simple double barrier with the same effective mass k_y. Thus, in this case we reproduce exactly the transmission obtained in [13], for the massive Dirac equation with $m = k_y$. Let us treat the triangular double barrier case when $v_2 < v_1$ and $v_2 > v_1$. In both cases, the transmission is plotted in Figure 8: In Figure 8a) $v_2 > v_1$ we distinguish

five different zones characterizing the behavior of the transmission coefficient :

- The first is determined by the greater effective mass, namely $\epsilon l_B < k_y l_B + \frac{d_1}{l_B}$.
- The second identifies with the lower Klein energy zone characterized by resonances and $k_y l_B + \frac{d_1}{l_B} < \epsilon l_B < v_1 l_B$. Here we have full transmission at some specific energies despite the fact that the particle energy is less than the height of the barrier. As d_1/l_B increases, the oscillations in the Klein zone get reduced. This strong reduction in the transmission in the Klein zone seem to suggest the potential suppression of the Klein tunneling as we increase d_1/l_B.
- The third zone $v_1 l_B < \epsilon l_B < v_2 l_B - k_y l_B - \frac{\mu l_B}{2}$ is a window where the transmission oscillates around the value of the total transmission.
- The fourth zone defined by $v_2 l_B - k_y l_B - \frac{\mu l_B}{2} < \epsilon l_B < v_2 l_B + k_y l_B + \frac{\mu l_B}{2}$ is a window where the transmission is almost zero.
- The fifth zone $\epsilon l_B > v_2 l_B + k_y l_B + \frac{\mu l_B}{2}$ contains oscillations, the transmission converges towards unity.

Contrary to the case $v_1 > v_2$, see Figure 8b) we distinguish fourth different zones characterizing the behavior of the transmission coefficient:

- Compared to Figure 8a), the behavior in the first zone is the same as in in Figure 8a).
- Concerning the zones $k_y l_B - \frac{d1}{l_B} < \epsilon l_B < v_2 l_B - k_y l_B - \frac{\mu l_B}{2}$ and $v_2 l_B + k_y l_B + \frac{\mu l_B}{2} < \epsilon l_B < v_1 l_B$ the transmission oscillates similarly to Figure 8a).
- In the zone $v_2 l_B - k_y l_B - \frac{\mu l_B}{2} < \epsilon l_B < v_2 l_B + k_y l_B + \frac{\mu l_B}{2}$, one can see that both curves start from zero transmission and oscillate while the valley gets wider as d_1/l_B decreases.
- Finally zone $\epsilon l_B > v_1 l_B$ the transmission oscillate to reach the total transmission.

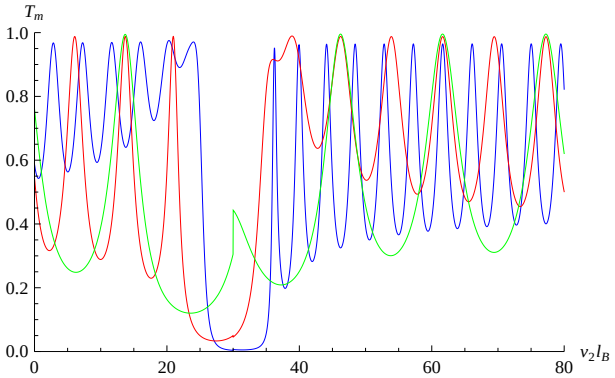

Figure 9: (Color online) Transmission probability T_m for the magnetic barrier as a function of potential $v_2 l_B$ with $\frac{d_1}{l_B} = 0.1$ color green, $\frac{d_1}{l_B} = 0.2$ color red, $\frac{d_1}{l_B} = 0.34$ color blue, $\frac{d_2}{l_B} = 1.5$, $\mu l_B = 4$, $k_y l_B = 2$, $v_1 l_B = 60$ and $\epsilon l_B = 30$. .

It is worth to analyze the transmission versus the potential $v_2 l_B$. In doing so, we choose a fixed value of d_1/l_B to present Figure 9. It is clear that two transmission curves increase while d_1/l_B decreases in the intermediate zone.

5 Conclusion

We have considered a model to describe over-barrier electron emission from the edge of monolayer graphene through a triangular electrostatic double barriers in addition to a magnetic field in graphene. To underline the behavior of our system, we have separately considered two parts: first including static barrier and second deal with magnetic barrier. In both cases, we have set the materials needed to analytically determine and numerically analyze the transmission probability. These have been done by solving the eigenvalue equation to end up with the solutions of the energy spectrum in terms of different physical parameters involved in the Hamiltonian system.

By using the continuity of the wavefunctions at the interfaces between different regions inside and outside the barriers we have ensured conservation of the local current density and derived the relevant transport coefficients of the present system. Specifically, using the transfer matrix method, we have analyzed the corresponding transmission coefficient and determined how the transmission probability is affected by various physical parameters. In particular for static barrier, the resonances were seen in different regions as well as the Klein tunneling effect.

Subsequently, we have analyzed the same system but this time by taking into account the presence of an inhomogeneous magnetic field. Using boundary conditions, we have split the energy into three domains and then calculated the transmission probability in each case. In each situation, we have discussed the transmission at resonances that characterize each region and stressed the importance of our results.

Acknowledgments

The generous support provided by the Saudi Center for Theoretical Physics (SCTP) is highly appreciated by all authors. AJ acknowledges partial support by King Faisal University while HB acknowledge the support of King Fahd University of Petroleum and minerals under research group project RGxxxx.

References

[1] K. S. Novoselov, A. K. Geim, S. V. Morozov, D. Jiang, Y. Zhang, S. V. Dubonos, I. V. Grigorieva and A. A. Firsov, Science 306, 666 (2004).

[2] N. Stander, B. Huard and D. Goldhaber-Gordon, Phys. Rev. Lett. 102, 026807 (2009).

[3] M. I. Katsnelson, K. S. Novoselov and A. K. Geim, Nature Phys. 2, 620 (2006).

[4] H. Sevincli, M. Topsakal and S. Ciraci, Phys. Rev. B 78, 245402 (2008).

[5] H. Sevincli, M. Topsakal and S. Ciraci, Phys. Rev. B 78, 245402 (2008).

[6] M. R. Masir, P. Vasilopoulos and F. M. Peeters, New J. Phys. 11, 095009 (2009).

[7] L. DellAnna and A. De Martino, Phys. Rev. B 79, 045420 (2009).

[8] S. Mukhopadhyay, R. Biswas and C. Sinha, Phys. Status Solidi B 247, 342 (2010).

[9] E. B. Choubabi, M. El Bouziani and A. Jellal, Int. J. Geom. Meth. Mod. Phys. 7, 909 (2010).

[10] H. Bahlouli, E. B. Choubabi, A. Jellal and M. Mekkaoui, J. Low Temp. Phys. 169, 51 (2012).

[11] A. Jellal and A. El Mouhafid, J. Phys. A: Math. Theo. 44, 015302 (2011).

[12] J. Tworzydlo, B. Trauzettel, M. Titov, A. Rycerz and C. W. J. Beenakker, Phys. Rev. Lett. 96, 246802 (2006).

[13] A. D. Alhaidari, H. Bahlouli and A. Jellal, Advances in Mathematical Physics 2012, ID 762908 (2012).

[14] H. Bahlouli, E.B. Choubabi, A. El Mouhafid and A. Jellal, Solid State Communications 151, 1309 (2011).

[15] A. Matulis, F. M. Peeters, P. Vasilopoulos, Phys. Rev. Lett. 72, 1518 (1994).

[16] M. Ramezani Masir, P. Vasilopoulos, F. M. Peeters, Phys. Rev. B 82, 115417 (2010).

[17] J. Tworzydlo, B. Trauzettel, M. Titov, A. Rycerz and C. W. J. Beenakker, Phys. Rev. Lett. 96, 246802 (2006).

[18] M. V. Berry and R. J. Modragon, Proc. R. Soc. London Ser. A 412, 53 (1987).

[19] M. Abramowitz and I. Stegum, Handbook of Integrabls, Se ries and Products, (Dover, New York, 1956).

[20] L. Gonzalez-Diaz and V. M. Villalba, Phys. Lett. A 352, 202 (2006).